

Transverse Current Generation by Circularly Polarized Light in Terahertz-Biased Semiconductor

Tomohiro Fujimoto,^{*} Yuta Murotani, Tomohiro Tamaya, Takayuki Kurihara, Natsuki Kanda[‡],
Changsu Kim, Jun Yoshinobu, Hidefumi Akiyama, Takeo Kato, and Ryusuke Matsunaga[†]

The Institute for Solid State Physics, The University of Tokyo, Kashiwa, Chiba 277-8581, Japan

^{*}fujimoto@issp.u-tokyo.ac.jp

[†]matsunaga@issp.u-tokyo.ac.jp

[‡]Present address: RIKEN Center for Advanced Photonics, RIKEN, 2-1 Hirosawa, Wako,
Saitama 351-0198, Japan

Abstract (600 characters).

Transverse current generation by circularly polarized light in biased matter has attracted considerable attention for studies of Floquet engineering and inverse spin Hall effect. Field-induced circular photogalvanic effect (FI-CPGE) also contributes to the current, but has been overlooked in many literatures. Using terahertz pulses as a bias field, we study the case of a prototypical semiconductor GaAs by two-dimensional Fourier analysis. We demonstrate the remarkable role of FI-CPGE resonantly enhanced near the band degeneracy, suggesting its potential to detect monopoles in momentum space. Our results provide a comprehensive understanding of the light-induced anomalous Hall effect.

Main text

Nonthermal control of matter using intense light fields has recently attracted tremendous interest in ultrafast optical science and condensed matter physics because nontrivial states can manifest themselves in nonequilibrium [1–3]. Of particular interest is the case driven by a circularly

polarized light (CPL); based on the Floquet theory, a periodic CPL field can be embedded in light-dressed states of electrons with an artificial gauge field and the associated Berry curvature [4]. The topologically nontrivial states of electrons under light illumination are expected to produce an anomalous Hall current to a bias field [5–10]. Beyond simple CPL, counterrotating bicircular light pulses [11–13] have also attracted growing interest as a way to impose a specific rotational symmetry on matter, which may also produce nontrivial states with finite Hall conductivity [14–16].

However, interpretation of the transverse current observed under CPL irradiation in a biased material requires special care. A representative example is the light-induced anomalous Hall effect in a two-dimensional (2D) Dirac system, which is theoretically anticipated to be a signature of the Floquet-topological insulating phase [5]. Although the light-induced transverse current in biased graphene was recently observed experimentally [17], theoretical analysis revealed that the Floquet-topological phase plays only a minor role in the current, and the current is dominated by the momentum asymmetry of photoexcited carriers [18], as schematically shown in Fig. 1(a). This process can be understood as a nominally second-order photocurrent generation by CPL due to broken inversion symmetry by a bias field, which we term the field-induced circular photogalvanic effect (FI-CPGE) [19]. As long as CPL and a bias field are applied to a material simultaneously, both the Hall current due to time-reversal symmetry breaking by CPL and the photocurrent due to inversion symmetry breaking by the bias field should contribute to the transverse current on the same footing [19]. Although most theoretical studies of Floquet engineering and light-field control of matter have considered only the former mechanism, a recent experiment has also demonstrated that the latter, FI-CPGE, is dominant in a three-dimensional Dirac semimetal [19]. FI-CPGE can be viewed as a helicity-dependent photovoltaic Hall response, which should occur quite generally even in centrosymmetric materials [20]. Therefore, for a comprehensive understanding of the light-induced anomalous Hall effect, the role of FI-CPGE must be experimentally clarified also in more conventional materials. A prototypical semiconductor GaAs has a well-defined bandgap and multiple valence bands involved in optical transitions, which will provide a general perspective for the interaction with light and bias fields.

Despite its simple and fundamental aspects, the microscopic mechanism of the photovoltaic Hall current in conventional semiconductors is complicated and highly nontrivial, which has stimulated recent theoretical studies [21–25] including an interest in Riemannian geometry [20]. The Floquet-topological phase transition predicted in gapless systems [5] can be ignored in semiconductor GaAs. Instead, spin-polarized carriers excited by CPL give rise to the transverse current as shown in Fig. 1(b), which we term the light-induced inverse spin Hall effect (LI-ISHE). LI-ISHE has been extensively studied in the field of spintronics using a static bias field and continuous-wave (CW) light [26–29]; however, the contribution of FI-CPGE has been neglected. To discriminate between FI-CPGE and LI-ISHE, time-resolved detection of the transient Hall conductivity *during* and *after* CPL pump pulse irradiation is pivotal because FI-CPGE occurs only *during* the pump, whereas LI-ISHE occurs even *after* the pump as long as the spin polarization survives [19, 30]. Using optical pump-terahertz (THz) probe spectroscopy, the ISHE of electrons in GaAs was observed *after* the pump, realizing a quantitative evaluation of the spin Hall conductivity spectrum [31]. The ISHE of holes has also been observed in a similar way in GaAs quantum wells at low temperature [32]. However, the transverse current *during* CPL irradiation in conventional semiconductors has not been investigated, despite its practical importance in more common situations using static bias and CW light. Although the previous study of a Dirac semimetal could elucidate the dominance of FI-CPGE based on the sign of $\sigma_{yx}(\omega)$ [19], such a qualitative factor can be used only in simple systems described by a 2-band model, and therefore it is not directly applicable to more general semiconductors. A new strategy for the quantitative evaluation of FI-CPGE and LI-ISHE must be developed for deeper insight into the fundamental nonlinear light–matter interaction related to the band topology, as well as for light energy harvesting in the photovoltaic response of biased materials.

In this Letter, we conduct optical pump-THz Faraday probe spectroscopy to investigate the transient photovoltaic Hall response in bulk semiconductor GaAs *during* irradiation with near-infrared (NIR) CPL pulses. Our 2D frequency-domain analysis successfully discriminated between LI-ISHE and FI-CPGE. We demonstrate the considerable role of the spectral filtering function inherent to optical pump-THz probe spectroscopy. Even though the detection of FI-CPGE is significantly suppressed by the spectral filter, we show that FI-CPGE dominates the observed signal for a large pump fluence and is enhanced near the bandgap, which agrees well with the

microscopic theory. This work presents a comprehensive understanding of the origins of the CPL-induced anomalous Hall current and develops a procedure to probe the band degeneracy point and the dispersion relation around it away from the Fermi level.

For sample preparation, we first grew 1.0 μm -thick non-doped GaAs (001) sandwiched between 1.7 μm -thick $\text{Al}_{0.19}\text{Ga}_{0.81}\text{As}$ protective layers using the molecular-beam epitaxy method on a non-doped GaAs substrate. The substrate was then removed by mechanical polishing and selective chemical etching over a diameter of 4 mm to make a free-standing sample suitable for transmission measurements. All the experiments were performed at room temperature, where the bandgap E_g is 1.42 eV. Figure 1(c) shows the configuration of the optical pump-THz Faraday probe spectroscopy setup. A Yb:KGW laser amplifier was used. The output beam was separated into three beams. One was converted into an NIR CPL pulse with a tunable pump photon energy $\hbar\Omega_{\text{pump}}$ between 1.38 eV and 1.56 eV using an optical parametric amplifier. The other two beams were used for THz pulse generation and for the gate pulse to detect the THz pulse in a GaP crystal. The incident THz pulse was linearly polarized in the x direction. We used a pair of wire-grid polarizers for the transmitted THz pulses to detect the y component originating from the transverse current in the sample, depending on the pump helicity [31]. The delay times t_1 and t_2 were scanned by changing the beam path lengths of the THz probe and NIR pump pulses, respectively. To extract the signal depending on the pump helicity, we evaluated the y component as the difference between the signals for left- and right-handed CPL. Detailed information about the experiment and analysis is available in the Supplemental Material [33].

The upper panel of Fig. 2(a) shows $E_x(t_1)$, the THz probe pulse waveform after transmitting the sample without a pump. The middle panel shows 2D plots of $E_y(t_1, t_2)$, the Faraday rotation signal induced by the CPL pump. Here, $\hbar\Omega_{\text{pump}}$ is 1.46 eV and the pump fluence is $16 \mu\text{J cm}^{-2}$, for which the E_y signal oscillates along the t_1 -axis. The bottom panel shows the data for a larger pump fluence of $210 \mu\text{J cm}^{-2}$. Remarkably, a distinct diagonally oscillating waveform was observed. The qualitative differences in the 2D plots between the weak and strong excitations suggest that the dominant origin of the CPL-induced THz Faraday rotation changes with pump fluence.

The 2D data in the middle panel of Fig. 2(a) is similar to the recently reported LI-ISHE in GaAs [31]. The E_y signal decays along the t_2 -axis with fast (200 fs) and slow (80 ps) components, which coincide well with the spin relaxation times of photoexcited holes [41] and electrons [42], respectively. Based on spectral analysis, the slowly decaying smaller signal has been well explained by LI-ISHE of spin-polarized electrons [31]. Similarly, the fast-decaying larger signal at $t_2 = 0$ ps in the middle panel is attributed to LI-ISHE of short-lived spin-polarized holes with stronger spin-orbit interaction [43]. By contrast, the diagonally oscillating signal in the bottom panel of Fig. 2(a) is similar to that of the recently reported FI-CPGE in a Dirac semimetal [19]. Therefore, the data suggests that the observed Faraday rotation signal may be dominated by LI-ISHE (FI-CPGE) in the weak (strong) excitation regime, as examined below.

To discuss LI-ISHE of holes and FI-CPGE, which temporally overlap in $E_y(t_1, t_2)$, we conducted a 2D-Fourier transform and plotted $|E_y(\omega_1, \omega_2)|$ in Fig. 2(b). In the 2D frequency domain, a single tilted ellipse at $\omega_2/2\pi \sim 0$ THz appears for the weaker excitation (left panel), while a second ellipse at $\omega_2/2\pi \sim -2.5$ THz appears for the stronger excitation (right panel). To understand these features, the nonlinear response functions of both processes were considered. In LI-ISHE, the pump pulse leaves spin-polarized carriers that respond to the bias field $E_x(t_1)$ with a finite Hall conductivity and decay along t_2 owing to spin relaxation. By contrast, FI-CPGE generates a photocurrent only at the arrival of the pump under the bias field, *i.e.*, at $t_2 = t_1$. Therefore, each response function can be modeled as

$$\sigma_{\text{LI-ISHE}}^{(3)}(t_1, t_2) = \Theta(t_2)e^{-\gamma_s t_2} \times \sigma_{\text{ISHE}}^{yx}(t_1) \quad (1)$$

$$\sigma_{\text{FI-CPGE}}^{(3)}(t_1, t_2) = \Theta(t_2)e^{-\Gamma t_2} \times \alpha_{\text{CPGE}}\delta(t_2 - t_1), \quad (2)$$

where $\Theta(t)$ is a step function, $\delta(t)$ is a delta function, and Γ and γ_s are the decay constants. $\sigma_{\text{ISHE}}^{yx}(t_1)$ represents the inverse spin Hall conductivity of holes. α_{CPGE} represents the efficiency of FI-CPGE. The last two quantities can be highly dependent on $\hbar\Omega_{\text{pump}}$, as discussed later. The essential difference between the two response functions is evident in the 2D frequency domain:

$$\sigma_{\text{LI-ISHE}}^{(3)}(\omega_1, \omega_2) = \sigma_{\text{ISHE}}^{yx}(\omega_1) \frac{\gamma_s}{\gamma_s - i\omega_2}, \quad (3)$$

$$\sigma_{\text{FI-CPGE}}^{(3)}(\omega_1, \omega_2) = \frac{\Gamma \alpha_{\text{CPGE}}}{\Gamma - i(\omega_1 + \omega_2)}. \quad (4)$$

Assuming that $\sigma_{\text{ISHE}}^{yx}(\omega_1)$ and α_{CPGE} are constant for simplicity, Eqs. (3) and (4) are schematically shown in Figs. 3(a) and 3(b), respectively. The responses of LI-ISHE and FI-CPGE peak at $\omega_2 = 0$ and $\omega_1 + \omega_2 = 0$, respectively. Note that the observed signal $E_y(\omega_1, \omega_2)$ in the experiment is not solely determined by the nonlinear conductivity in Eq. (3) or (4) because the detectable spectral region can be restricted by other extrinsic factors: the probe pulse spectrum $E_x^{\text{bias}}(\omega_1)$, pump pulse envelope spectrum $I^{\text{pump}}(\omega_2)$ [33], and propagation function $G(\omega_1 + \omega_2)$ that relates the transverse current J_y to the detected electric field E_y . Although the precise form of $G(\omega_1 + \omega_2)$ is difficult to evaluate quantitatively because it is sensitive to the geometry of the optical system, $G(\omega_1 + \omega_2)$ necessarily produces a notch downward to the right along the line of $\omega_1 + \omega_2 = 0$, where the detection efficiency is precisely zero. This is a consequence of diffraction. The DC-limit electromagnetic wave does not propagate in free space; thus, it is never detected in noncontact THz spectroscopy [38]. Figure 3(c) summarizes the available spectral region, where two ellipses appear as a result of spectral filtering. Considering the extrinsic filter, we phenomenologically calculated the expected signals in the 2D temporal and frequency domains originating from LI-ISHE and FI-CPGE, as plotted in Figs. 3(d) and 3(e), respectively, which reproduce the experimental data in Figs. 2(a) and 2(b) very well. This confirmed that the observed signal of the CPL-induced THz Faraday rotation was dominated by LI-ISHE (FI-CPGE) at small (large) pump fluence.

It should be emphasized that the two ellipses observed in the stronger pump in Fig. 2(b) are just the “tails” of FI-CPGE. The peak of FI-CPGE exists along $\omega_1 + \omega_2 = 0$, but the propagation function $G(\omega_1 + \omega_2)$ prevents this main part from detection. Nevertheless, the experiment showed that the small tails of FI-CPGE can dominate the THz signal under certain conditions, which reveals the significance of FI-CPGE, although this has been disregarded in many studies. FI-CPGE signal would appear much more efficiently in contact-type measurements such as conventional DC transport and on-chip THz spectroscopy [17]. In other words, THz spectroscopy is suitable for studying LI-ISHE with efficient suppression of the other contributions from FI-CPGE.

While the lower ellipse at $\omega_2/2\pi \sim -2.5$ THz can be solely attributed to FI-CPGE, the upper ellipse at $\omega_2/2\pi \sim 0$ THz can include both LI-ISHE and FI-CPGE signals. To fully understand the dependence on pump fluence, we integrated the two ellipse signals separately and plotted the

current amplitude A_y as a function of pump fluence, as shown in Fig. 3(f) [33]. In contrast to the simple linearity of the lower ellipse, the upper ellipse saturates in the moderate fluence region ($50\text{--}100 \mu\text{J cm}^{-2}$) and increases again for larger fluences ($>100 \mu\text{J cm}^{-2}$). This nonmonotonic behavior is consistent with the dominant contribution of LI-ISHE (FI-CPGE) for weaker (stronger) excitation. LI-ISHE originates from the Hall conductivity of photoexcited carriers but is accompanied by a longitudinal Drude response, which significantly suppresses the penetration of the incident THz wave as the carrier density increases for stronger excitation. The dashed line in Fig. 3(f) shows the modeled fluence dependence of LI-ISHE accounting for this suppression [33]. By contrast, FI-CPGE is a field-assisted generation of photocurrent, which is much more robust against pump fluence unless the interband absorption saturates. Therefore, the upper ellipse signal was also dominated by FI-CPGE in the strong excitation regime, even though the main part of FI-CPGE was filtered out.

Next, we discuss the dependence of LI-ISHE and FI-CPGE on pump photon energy. Figures 4(a) and 4(b) show the lower and upper ellipse signals, A_y , as a function of $\hbar\Omega_{\text{pump}}$, which are dominated by LI-ISHE and FI-CPGE, respectively. Both signals are strongly enhanced near the bandgap. We also calculated $\sigma_{\text{LI-ISHE}}^{(3)}$ and $\sigma_{\text{FI-CPGE}}^{(3)}$ from the microscopic model based on the 6-band Kane Hamiltonian [33], according to the third-order susceptibility derived in a pioneering work [25]. The results of our calculations for GaAs in Figs. 4(a) and 4(b) agree well with the experimental data, including the fact that the peak of FI-CPGE is shifted to a higher energy than that of LI-ISHE. This difference is attributed to the microscopic origin of the current. LI-ISHE is driven by the Berry curvature of photoexcited holes [43], which is divergently enhanced at the valence band maximum where light-hole (LH) and heavy-hole (HH) bands touch as shown in Fig. 4(c) [44]. Such a divergent enhancement of LI-ISHE for varying $\hbar\Omega_{\text{pump}}$ is not expected for systems with no band touching point [20], and thus can be used to experimentally identify band degeneracy. By contrast, FI-CPGE originates from the third-order nonlinear interaction involving interband transitions between LH, HH, and conduction bands (CB), as shown in Fig. 4(d). In this work, we used the THz probe pulse centered at $\omega_{\text{probe}}/2\pi=1.2 \text{ THz}$, which resonates with the LH–HH transition at finite momenta near the Γ -point. Then, a pump pulse with $\hbar\Omega_{\text{pump}}$ slightly higher than the bandgap can make all three optical transitions in Fig. 4(d) resonant to the real states

of LH, HH, and CB without resorting to virtual states. Thus, FI-CPGE is resonantly enhanced slightly above the band degeneracy point, which depends on the frequency of the bias field, ω_{probe} , and the CB dispersion relation. The remarkable enhancement of FI-CPGE demonstrated in this study has important implications. Because FI-CPGE is described by an asymmetric momentum distribution of photocarriers [18], one might intuitively assume that FI-CPGE should be reduced near the band edge because of less joint density of states and vanishingly small group velocity. However, this study clearly shows that FI-CPGE is resonantly enhanced toward the band edge as long as the nearly degenerate bands are involved in the optical transitions. This result suggests that FI-CPGE plays a non-negligible role in the light-induced anomalous Hall effect, not only in simple Dirac systems [18, 19] but also in more general materials such as GaAs, particularly in contact-type measurements.

In summary, we demonstrated that the microscopic origins of the CPL-induced anomalous Hall response in GaAs can be resolved by LI-ISHE and FI-CPGE using 2D Fourier analysis based on the THz bias field. Although the spectral filtering inherent to THz spectroscopy suppresses the detection efficiency of FI-CPGE, it can be strong enough to dominate the signal when the degenerate band structure is involved in the optical transition. The results shed light on the interpretation of the CPL-induced anomalous Hall effect and helicity-dependent photovoltaic Hall response in general materials. Furthermore, band degeneracy is directly related to the presence of a topological quantity, called monopole charge, which generates a divergent Berry curvature [44]. Recently, second-order optical responses have attracted considerable attention as a probe of topological quantities in materials with broken inversion symmetry [45–48]. In contrast, third-order optical responses, including LI-ISHE and FI-CPGE, emerge even in centrosymmetric materials. This work shows that band degeneracy points can be sensitively detected by LI-ISHE with a wavelength-tunable light source. In addition, FI-CPGE with a finite-frequency bias field can provide information on the dispersion relation around the degeneracy point. Our results open a new pathway for investigating the monopole charges hidden in centrosymmetric materials.

Acknowledgements

This work was supported by JST FOREST (Grant No. JPMJFR2240), JST PRESTO (Grants No. JPMJPR2006, and No. JPMJPR2107), JST CREST (Grant No. JPMJCR20R4), and JSPS

KAKENHI (Grants No. JP24K00550, and No. JP24K16988, and No. JP20K22478). R.M. acknowledges support from MEXT Quantum Leap Flagship Program (MEXT Q-LEAP, Grant No. JPMXS0118068681). R.M. and T.F. conceived the project. C.K., T.F., and H.A. fabricated the sample. T.F., Y.M., and N.K. developed the pump-probe spectroscopy system with the help of T.Kurihara, J.Y., and R.M. T.F. performed the experiment and analyzed the data with help of Y.M. T.F. conducted theoretical calculation with help of Y.M, T.T., and T.Kato. All the authors discussed the results. T.F. and R.M. wrote the manuscript with substantial feedback from Y.M. and all the co-authors.

References

1. A. de la Torre, D. M. Kennes, M. Claassen, S. Gerber, J. W. McIver, and M. A. Sentef, Colloquium: Nonthermal pathways to ultrafast control in quantum materials. *Rev. Mod. Phys.* **93**, 041002 (2021).
2. C. Bao, P. Tang, D. Sun, and Shuyun Zhou, Light-induced emergent phenomena in 2D materials and topological materials. *Nat. Rev. Phys.* **4**, 33 (2021).
3. M. Borsch, M. Meierhofer, R. Huber, and M. Kira, Lightwave electronics in condensed matter. *Nat. Rev. Mater.* **8**, 668 (2023).
4. T. Oka and S. Kitamura, Floquet Engineering of Quantum Materials. *Annu. Rev. Condens. Matter Phys.* **10**, 387 (2019).
5. T. Oka and H. Aoki, Photovoltaic Hall effect in graphene. *Phys. Rev. B* **79**, 081406(R) (2009).
6. X. Wang, E. Ronca, and M.A. Sentef, Cavity quantum electrodynamical Chern insulator: Towards light-induced quantized anomalous Hall effect in graphene. *Phys. Rev. B* **99**, 235156 (2019).
7. M. Nuske, L. Broers, B. Schulte, G. Jotzu, S. A. Sato, A. Cavalleri, A. Rubio, J. W. McIver, and L. Mathey, Floquet dynamics in light-driven solids. *Phys. Rev. Research* **2**, 043408 (2020).
8. P. X. Nguyen and W.-K. Tse, Photoinduced anomalous Hall effect in two-dimensional transition metal dichalcogenides. *Phys. Rev. B* **103**, 125420 (2021).
9. Y. Hirai, S. Okumura, N. Yoshikawa, T. Oka, and R. Shimano, Floquet Weyl states at one-photon resonance: An origin of nonperturbative optical responses in three-dimensional materials. *Phys. Rev. Research* **6**, L012027 (2024).

10. N. Yoshikawa, Y. Hirai, K. Ogawa, S. Okumura, K. Fujiwara, J. Ikeda, T. Koretsune, R. Arita, A. Mitra, A. Tsukazaki, T. Oka, and R. Shimano, Light-induced chiral gauge field in a massive 3D Dirac electron system. arXiv:2209.11932.
11. I. Tyulnev, Á. Jiménez-Galán, J. Poborska, L. Vamos, P. St. J. Russell, F. Tani, O. Smirnova, M. Ivanov, R. E. F. Silva, and J. Biegert, Valleytronics in bulk MoS₂ with a topologic optical field. *Nature* **628**, 746 (2024).
12. S. Mitra, Á. Jiménez-Galán, M. Aulich, M. Neuhaus, R. E. F. Silva, V. Pervak, M. F. Kling, and S. Biswas. *Nature* **628**, 752 (2024).
13. K. Ogawa, N. Kanda, Y. Murotani, and R. Matsunaga, Programmable generation of counterrotating bicircular light pulses in the multi-terahertz frequency range. *Nat. Commun.* **15**, 6310 (2024).
14. Á. Jiménez-Galán, R. E. F. Silva, O. Smirnova, and M. Ivanov, Lightwave control of topological properties in 2D materials for sub-cycle and non-resonant valley manipulation. *Nat. Photon.* **14**, 728 (2020).
15. T. V. Trevisan, P. V. Arribi, O. Heinonen, R.-J. Slager, and P. P. Orth, Bicircular Light Floquet Engineering of Magnetic Symmetry and Topology and Its Application to the Dirac Semimetal Cd₃As₂. *Phys. Rev. Lett.* **128**, 066602 (2022).
16. N. Arakawa and K. Yonemitsu, Symmetry-protected difference between spin Hall and anomalous Hall effects of a periodically driven multiorbital metal. *Commun. Phys.* **6**, 43 (2023).
17. J. W. McIver, B. Schulte, F.-U. Stein, T. Matsuyama, G. Jotzu, G. Meier, and A. Cavalleri, Light-induced anomalous Hall effect in graphene. *Nat. Phys.* **16**, 38 (2020).
18. S. A. Sato, J. W. McIver, M. Nuske, P. Tang, G. Jotzu, B. Schulte, H. Hübener, U. De Giovannini, L. Mathey, M. A. Sentef, A. Cavalleri, and A. Rubio, Microscopic theory for the light-induced anomalous Hall effect in graphene. *Phys. Rev. B* **99**, 214302 (2019).
19. Y. Murotani, N. Kanda, T. Fujimoto, T. Matsuda, M. Goyal, J. Yoshinobu, Y. Kobayashi, T. Oka, S. Stemmer, and R. Matsunaga, Disentangling the Competing Mechanisms of Light-Induced Anomalous Hall Conductivity in Three-Dimensional Dirac Semimetal. *Phys. Rev. Lett.* **131**, 096901 (2023).
20. J. Ahn, G.-Y. Guo, N. Nagaosa, and A. Vishwanath, Riemannian geometry of resonant optical responses. *Nat. Phys.* **18**, 290 (2022).

21. C. Aversa and J. E. Sipe, Nonlinear optical susceptibilities of semiconductors: Results with a length-gauge analysis. *Phys. Rev. B* **52**, 14636 (1995).
22. X. Dai and F.-C. Zhang, Light-induced Hall effect in semiconductors with spin-orbit coupling. *Phys. Rev. B* **76**, 085343 (2007).
23. K. S. Virk and J. E. Sipe, Optical Injection and Terahertz Detection of the Macroscopic Berry Curvature. *Phys. Rev. Lett.* **107**, 120403 (2011).
24. F. Yang and R.-B. Liu, Nonlinear optical response induced by non-Abelian Berry curvature in time-reversal-invariant insulators. *Phys. Rev. B* **90**, 245205 (2014).
25. B. M. Fregoso, Bulk photovoltaic effects in the presence of a static electric field. *Phys. Rev. B* **100**, 064301 (2019); *ibid* **102**, 059901 (2020).
26. M. I. Miah, Observation of the anomalous Hall effect in GaAs. *J. Phys. D: Appl. Phys.* **40**, 1659 (2007).
27. C. M. Yin, N. Tang, S. Zhang, J. X. Duan, F. J. Xu, J. Song, F. H. Mei, X. Q. Wang, B. Shen, Y. H. Chen, J. L. Yu, and H. Ma, Observation of the photoinduced anomalous Hall effect in GaN-based heterostructures. *Appl. Phys. Lett.* **98**, 122104 (2011).
28. J. L. Yu, Y. H. Chen, C. Y. Jiang, Y. Liu, H. Ma, and L. P. Zhu, Observation of the photoinduced anomalous Hall effect spectra in insulating InGaAs/AlGaAs quantum wells at room temperature. *Appl. Phys. Lett.* **100**, 142109 (2012).
29. N. Okamoto, H. Kurebayashi, T. Trypiniotis, I. Farrer, D. A., Ritchie, E. Saitoh, J. Sinova, J. Mašek, T. Jungwirth, and C. H.W. Barnes, Electric control of the spin Hall effect by intervalley transitions, *Nat. Mater.* **13**, 932 (2014).
30. Y. Murotani, N. Kanda, T. Fujimoto, T. Matsuda, M. Goyal, J. Yoshinobu, Y. Kobayashi, T. Oka, S. Stemmer, and R. Matsunaga, Anomalous Hall Transport by Optically Injected Isospin Degree of Freedom in Dirac Semimetal Thin Film. *Nano Lett.* **24**, 222 (2024).
31. T. Fujimoto, T. Kurihara, Y. Murotani, T. Tamaya, N. Kanda, C. Kim, J. Yoshinobu, H. Akiyama, T. Kato, and R. Matsunaga, Observation of Terahertz Spin Hall Conductivity Spectrum in GaAs with Optical Spin Injection. *Phys. Rev. Lett.* **132**, 016301 (2024).
32. S. Priyadarshi, K. Pierz, and M. Bieler, Detection of the Anomalous Velocity with Subpicosecond Time Resolution in Semiconductor Nanostructures, *Phys. Rev. Lett.* **115**, 257401 (2015).

33. See Supplemental Material at [http:](http://) for sample preparation, experimental methods, and analysis, and theoretical calculation, which includes Refs. [34–39].
34. C.-H. Lu, Y.-J. Tsou, H.-Y. Chen, B.-H. Chen, Y.-C. Cheng, S.-D. Yang, M.-C. Chen, C.-C. Hsu, and A. H. Kung, Generation of intense supercontinuum in condensed media, *Optica* **1**, 400 (2014).
35. N. Kanda, N. Ishii, J. Itatani, and R. Matsunaga, Optical parametric amplification of phase-stable terahertz-to-midinfrared pulses studied in the time domain, *Opt. Express* **29**, 3479 (2021).
36. N. Kanda, K. Konishi, and M. Kuwata-Gonokami, Terahertz wave polarization rotation with double layered metal grating of complimentary chiral patterns, *Opt. Express* **15**, 11117 (2007).
37. T. Matsuda, T. Higo, T. Koretsune, N. Kanda, Yoshua Hirai, Hanyi Peng, Takumi Matsuo, Naotaka Yoshikawa, Ryo Shimano, S. Nakatsuji, and R. Matsunaga, Ultrafast dynamics of intrinsic anomalous Hall effect in the topological antiferromagnet Mn_3Sn , *Phys. Rev. Lett.* **130**, 126302 (2023).
38. H. Němec, F. Kadlec, and P. Kužel, Methodology of an optical pump-terahertz probe experiment: An analytical frequency-domain approach. *J. Chem. Phys.* **117**, 8454 (2002).
39. R. A. Kaindl, D. Hägele, M. A. Carnahan, and D. S. Chemla, Transient terahertz spectroscopy of excitons and unbound carriers in quasi-two-dimensional electron-hole gases, *Phys. Rev. B* **79**, 045320 (2009).
40. B. M. Fregoso, R. A. Muniz and J. E. Sipe, Jerk Current: A Novel Bulk Photovoltaic Effect. *Phys. Rev. Lett.* **121**, 176604 (2018).
41. D. J. Hilton and C. L. Tang, Optical Orientation and Femtosecond Relaxation of Spin-Polarized Holes in GaAs. *Phys. Rev. Lett.* **89**, 146601 (2002).
42. S. Oertel, J. Hübner, and M. Oestreich, High temperature electron spin relaxation in bulk GaAs. *Appl. Phys. Lett.* **93**, 132112 (2008).
43. J. Wunderlich, B. Kaestner, J. Sinova, and T. Jungwirth, Experimental Observation of the Spin-Hall Effect in a Two-Dimensional Spin-Orbit Coupled Semiconductor System, *Phys. Rev. Lett.* **94**, 047204 (2005).
44. S. Murakami, N. Nagaosa, and S.-C. Zhang, Dissipationless Quantum Spin Current at Room Temperature. *Science* **301**, 1348 (2003).
45. T. Morimoto and N. Nagaosa, Topological nature of nonlinear optical effects in solids. *Sci. Adv.* **2**, e1501524 (2016).

46. S. Patankar, L. Wu, B. Lu, M. Rai, J. D. Tran, T. Morimoto, D. E. Parker, A. G. Grushin, N. L. Nair, J. G. Analytis, J. E. Moore, J. Orenstein, and D. H. Torchinsky, Resonance-enhanced optical nonlinearity in the Weyl semimetal TaAs. *Phys. Rev. B* **98**, 165113 (2018).
47. F. de Juan, A. G. Grushin, T. Morimoto, and J. E. Moore, Quantized circular photogalvanic effect in Weyl semimetals. *Nat. Commun.* **8**, 15995 (2017).
48. D. Rees, K. Manna, B. Lu, T. Morimoto, H. Borrmann, C. Felser, J. E. Moore, D. H. Torchinsky, and J. Orenstein, Helicity-dependent photocurrents in the chiral Weyl semimetal RhSi. *Sci. Adv.* **6**, eaba0509 (2020).

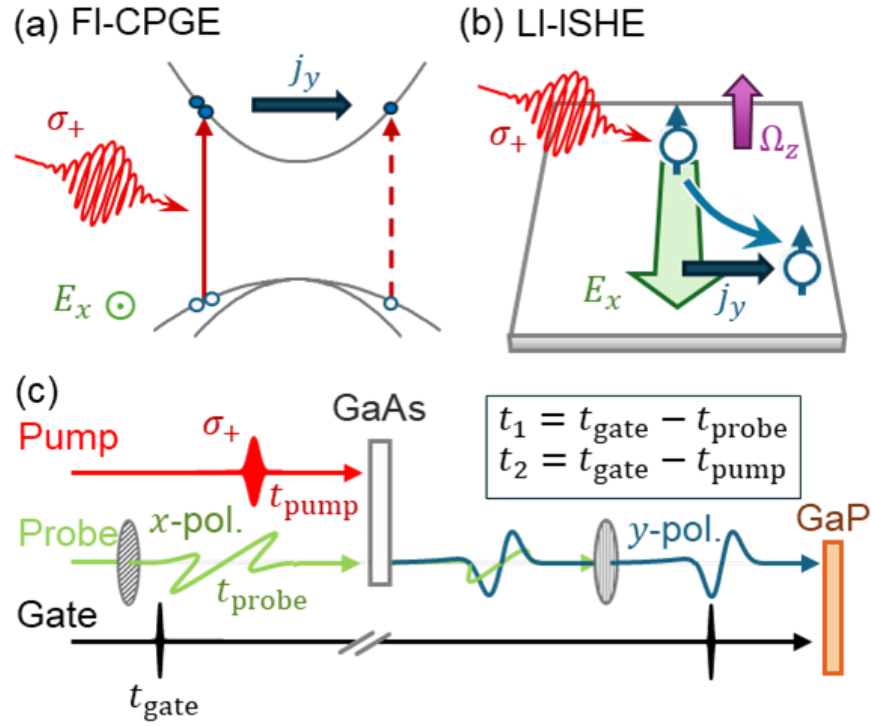


FIG. 1. (a)(b) Origins of the light-induced anomalous Hall effect or photovoltaic Hall response in semiconductors: FI-CPGE due to the momentum asymmetry of photoexcited carriers and LI-ISHE driven by the Berry curvature. (c) Configuration of circularly polarized NIR pump-THz Faraday probe spectroscopy. t_1 and t_2 are scanned by changing the optical beam path lengths of the THz probe and NIR pump pulses, respectively.

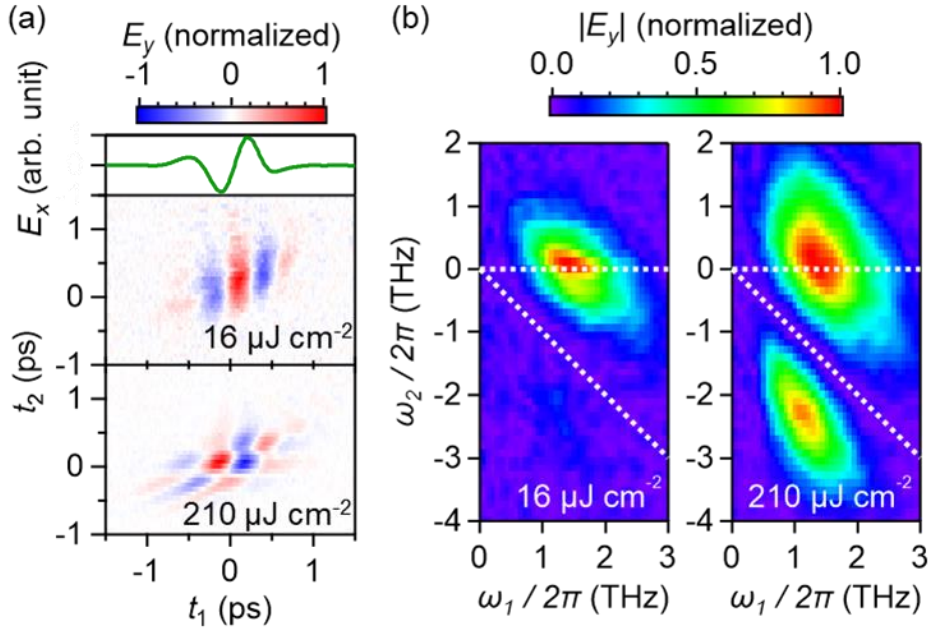


FIG. 2. (a) THz probe pulse waveform $E_x(t_1)$ after transmission (top). 2D plots of THz Faraday rotation signal $E_y(t_1, t_2)$ induced by CPL for fluences of $16 \mu\text{J cm}^{-2}$ (center) and $210 \mu\text{J cm}^{-2}$ (bottom). (b) 2D Fourier plots of the Faraday rotation signal $|E_y(\omega_1, \omega_2)|$ for fluences of $16 \mu\text{J cm}^{-2}$ (left) and $210 \mu\text{J cm}^{-2}$ (right). The horizontal (diagonal) dotted lines correspond to $\omega_2 = 0$ ($\omega_1 + \omega_2 = 0$).

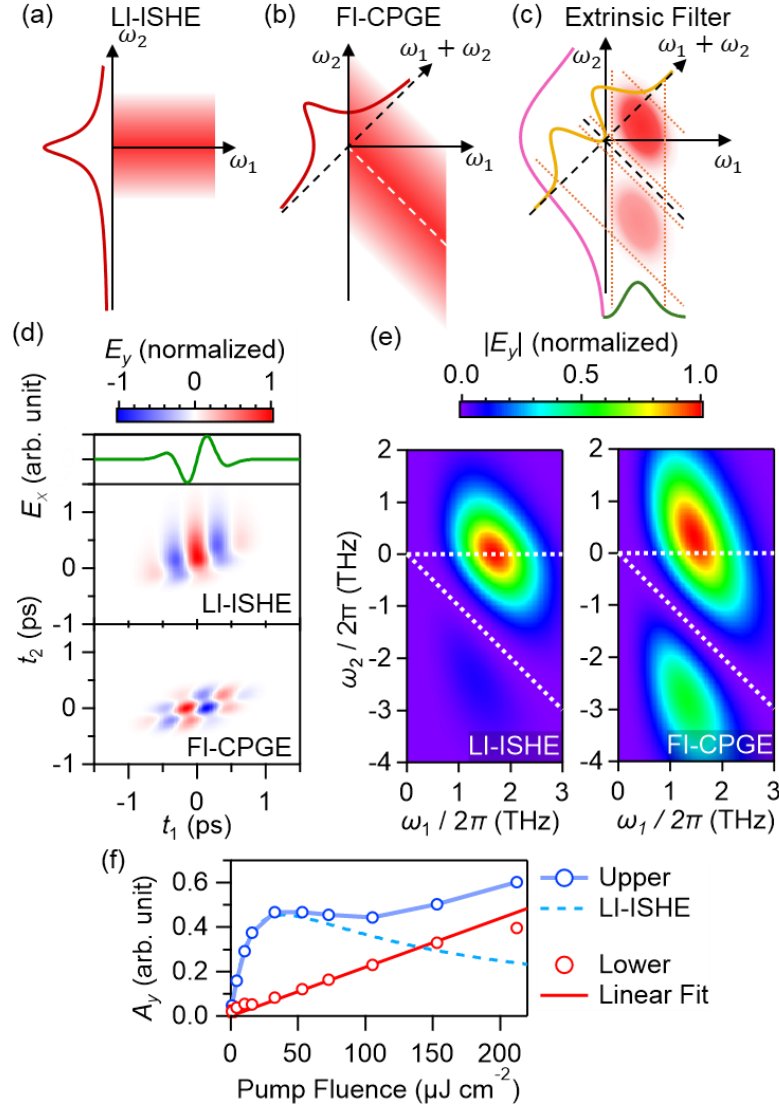


FIG. 3. 2D Response functions of (a) LI-ISHE and (b) FI-CPGE modeled using Eqs. (3) and (4), respectively. (c) Extrinsic filters limiting the detectable spectral regions in optical pump-THz probe spectroscopy: probe spectrum (green), pump envelope spectrum (pink), and propagation function (orange). The diagonal lines in (b) and (c) correspond to $\omega_1 + \omega_2 = 0$. (d) THz probe pulse waveform $E_x(t_1)$ used for the calculation (top). 2D plots of the calculated Faraday rotation signal $E_y(t_1, t_2)$ for LI-ISHE (middle) and FI-CPGE (bottom). (e) 2D Fourier plots of the Faraday rotation signal $|E_y(\omega_1, \omega_2)|$ for LI-ISHE (left) and FI-CPGE (right). The horizontal (diagonal) dotted lines correspond to $\omega_2 = 0$ ($\omega_1 + \omega_2 = 0$). (f) Pump fluence dependence of the current amplitude for the upper and lower ellipses in the 2D Fourier plots in the experiment.

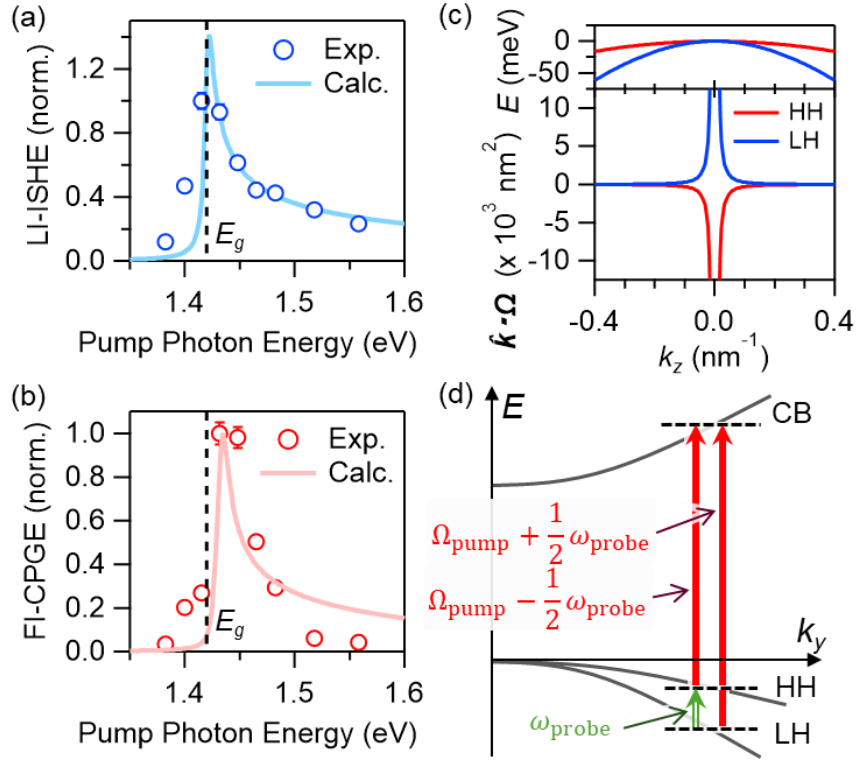


FIG. 4. Pump photon energy dependence of the current amplitudes for (a) LI-ISHE and (b) FI-CPGE, respectively, with a fixed fluence of $100 \mu\text{J cm}^{-2}$. The markers and curves show the results of experiments and calculations, respectively. (c) Calculated band structure near the band edge in GaAs (top) and the Berry curvature (bottom). (d) Diagram of nonlinear interactions involving LH, HH, and CB.